SAND75-0315

SINGLE-ATOM MASS SPECTROSCOPIES: THE ATOM-PROBE AND IMAGING FIELD-DESORPTION MASS SPECTROMETER

J. A. PANITZ

Sandia Laboratories

Issued by Sandia Laboratories, operated for the United States Energy Research and Development Administration by Sandia Corporation.

SAND 75-0315

J. A. Panitz
Sandia Laboratories, Albuquerque, New Mexico 87115

The atom-probe and imaging field-desorption mass spectrometer (called single-atom mass spectroscopies, or SAMS) occupy a unique place among the methods currently available for surface characterization. Unlike the more conventional electron spectroscopies (Auger, appearance potential, and photoelectron), they are truly surface-sensitive, sampling the constituent species of only the first atomic layer, and since they employ mass-spectrometric means for species identification, they can directly detect all surface species, including hydrogen. Whereas surface structure can only be dtermined on a gross average scale by diffraction methods, the single-atom spectroscopies, incorporating the magnification advantage of the field-ion microscope, can determine the location of individual surface species and detail (on an atomic scale) the extent of localized lattic imperfections. Since such techniques can controllably remove each atom layer of a specimen to expose the one underneath, depth profiling of surface species can be achieved with a resolution unequaled by any other method. Moreover, since species abundance can usually be determined by direct counting of detected species, only detection efficiency (an experimentally determinable parameter), and not theoretical estimates of cross sections or matrix contributions, will determine compositional accuracy. As a result, the single-atom spectroscopies can provide a more quantitative picture of surface and near-surface composition and structure then previously available. In the following pages these techniques will be outlined with particular emphasis on the more recent imaging field-desorption method developed at Sandia Laboratories.

Single-Atom Mass Spectroscopies are unique in that they provide:

1. Surface morphology and structure with angstrom resolution.

2. The identity of all surface species with the ability to preselect one surface atom for analysis, or determine the crystallographic distribution of one species on the surface.

3. Depth profiling of species with angstrom resolution. When combined with (2), above, complete three-dimensional (surface and depth) profiles of a pre-selected species (e.g., hydrogen or helium) can be obtained with angstrom resolution.

4. Very high detection sensitivity (10^{-15} monolayers for any species).

THE ATOM-PROBE FIELD-ION MICROSCOPE[1] (opposite, left) determines the identify of a surface species producing a preselelected ion-image spot on the screen of a field-ion microscope. This is accomplished by field-desorbing (removing) a monolayer of the substrate and allowing only the species of interest to pass into a mass spectrometer.

THE IMAGING FIELD-DESORPTION MASS SPECTROMETER[2] (opposite, right) determines the complete crystallographic distribution of a preselected surface species by field-desorbing (removing) a monolayer of the substrate and photographing the phosphor screen of a detector activated (time-gated) coincidently with the arrival of the selected species. Since a field-ion image is not used for species selection, any surface species can be preselected, even those (like hydrogen) which are not imaged in the field-ion microscope.

---

[1] E. W. Muller, J. A. Panitz, S. B. McLane, Rev. Sci. Instr. 39, 83 (1968).

[2] J. A. Panitz, J. Vac. Sci. Technol. 11, 206 (1974).

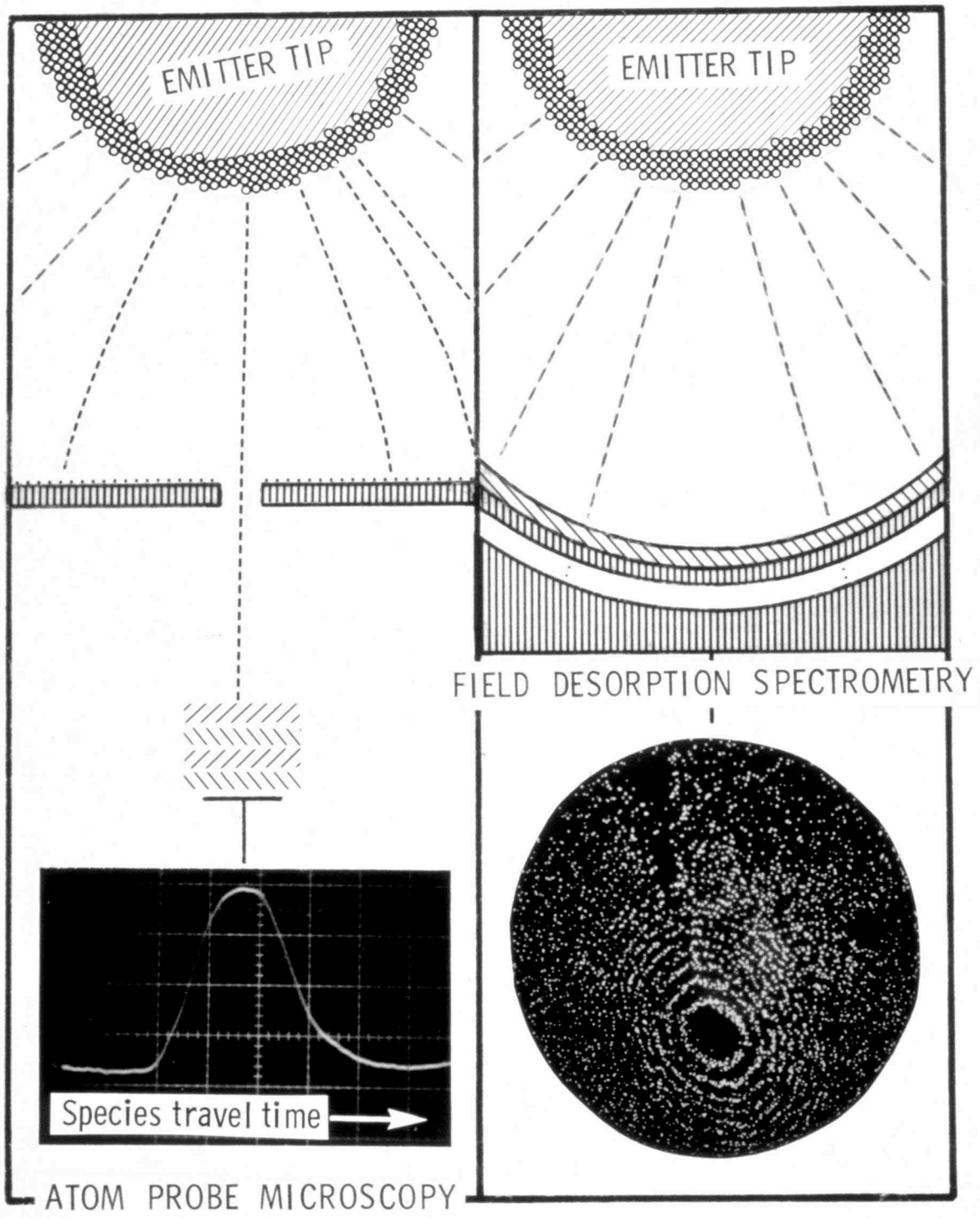
EMITTER TIP
EMITTER TIP
FIELD DESORPTION SPECTROMETRY
Species travel time
ATOM PROBE MICROSCOPY

THE IMAGING FIELD-DESORPTION MASS SPECTROMETER

A 10 cm atom-probe[1] with a unique spherical, Channel-Electron-Multiplier-Array (CEMA) detector is the basis of the instrumentation (opposite). A sharp, needle-like specimen at the base of a "cold-finger" is biased, and pulsed to field-desorb its surface. The following information can be obtained during each desorption pulse.

1. The mass spectrum (identity) of all surface species within the imaged area. (Their sequential arrival at the CEMA is observed on an oscilloscope whose sweep is initiated by the desorption pulse).
2. The mass spectrum (identity) of all surface species within several localized regions of the surface. (The output of several apertured photomultipliers is recorded as in (1) above.)
3. The crystallographic distribution of one preselected surface species. (A "digital delay" activates the CEMA detector at a unique time (the preselected species travel-time) relative to the desorption pulse. The fiberoptic screen of the detector is photographed to record the resulting distribution.)

[1] J. A. Panitz, Rev. Sci. Instr. 44, 1034 (1973).

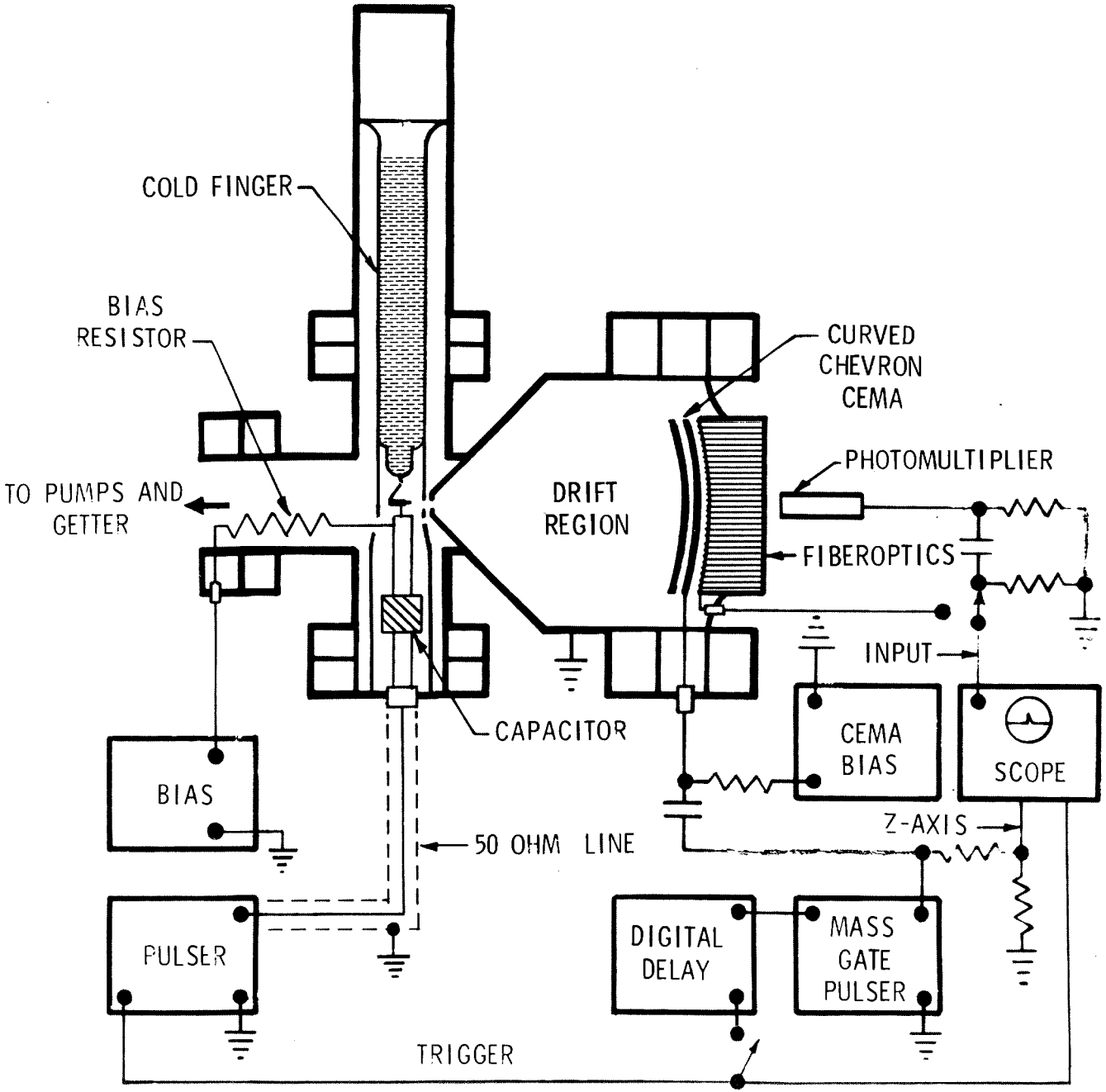
COLD FINGER
BIAS RESISTOR
TO PUMPS AND GETTER
CURVED CHEVRON CEMA
PHOTOMULTIPLIER
DRIFT REGION
FIBEROPTICS
INPUT
CAPACITOR
CEMA BIAS
SCOPE
BIAS
50 OHM LINE
Z-AXIS
PULSER
DIGITAL DELAY
MASS GATE PULSER
TRIGGER

A FIELD-ION IMAGE (opposite, upper) is used in Field-Desorption Mass Spectrometry to obtain substrate orientation since the ion-imaging process is non-destructive. However, only protruding (edge or "kink-site") atoms of the specimen are seen because the electric-field above other atoms will be too small to ionize the background "imaging" gas (usually helium).

GATED-DESORPTION images are obtained by field-desorbing (removing) substrate and adsorbed atoms from the surface as positive ions. Each species arrives at a detector at a unique time. If the detector is activated (time-gated) coincidently with the arrival of only one species, only it will be detected. Photographing the phosphor screen of the detector produces gated-desorption images (opposite, below), which show the distribution of each species on the surface.

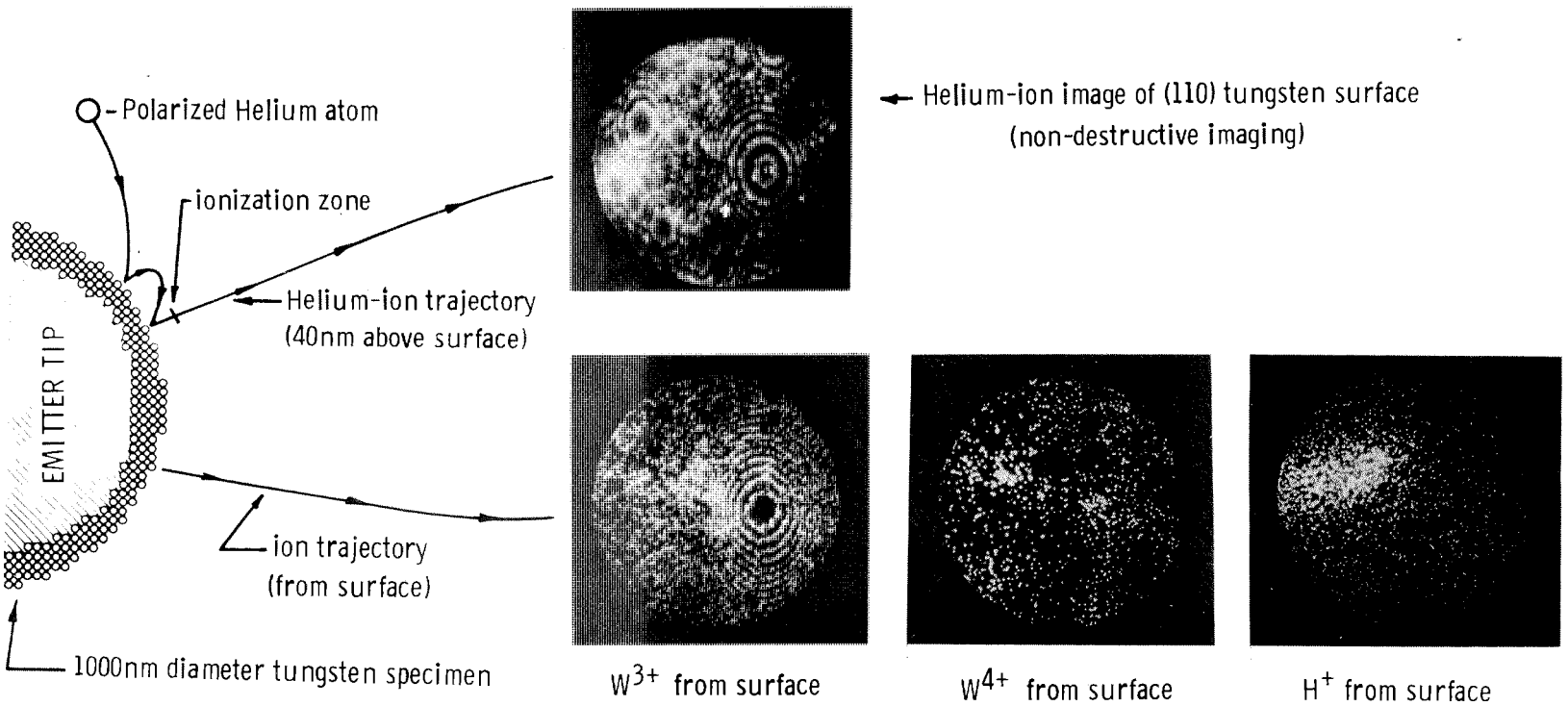
Polarized Helium atom
ionization zone
Helium-ion trajectory
(40nm above surface)
EMITTER TIP
ion trajectory
(from surface)
1000nm diameter tungsten specimen
Helium-ion image of (110) tungsten surface
(non-destructive imaging)
W3+ from surface
W4+ from surface
H+ from surface

HYDROGEN SEGREGATION ON IRIDIUM AT $78^{o}K$

If a carbon impurity is present in an iridium lattice, hydrogen will segregate to the impurity, producing a characteristic gated-desorption image of H^{+} (opposite, below). A field-ion image (opposite, above) is used to obtain the orientation of the substrate lattice. By alternately time-gating for carbon and then hydrogen, highly localized adsorption of hydrogen at the carbon impurity is demonstrated.

HYDROGEN SEGREGATION ON IRIDIUM AT 78°K

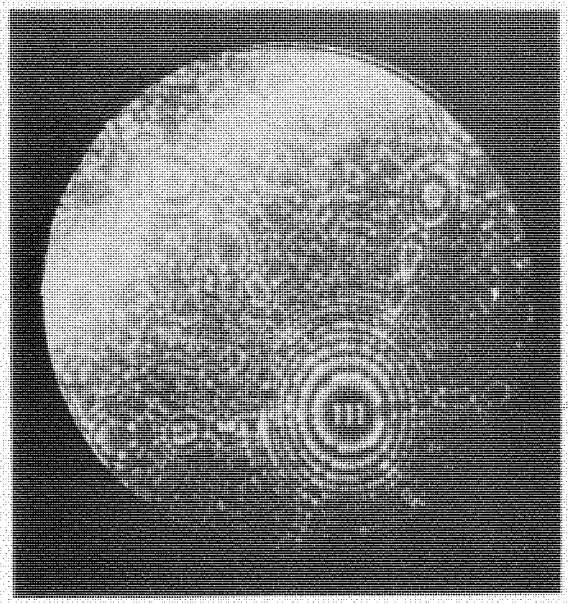

Helium-ion image of surface

2152074

H^+ from surface

(Segregation at two carbon impurity clusters in surface)

FIELD-ADSORPTION OF HELIUM AND NEON ON TUNGSTEN AT 78°K

The high electric field at the specimen surface (prior to field-desorption) encourages field-induced binding of noble gases. These field-adsorbed gases produce characteristic gated-desorption images* (top, right; bottom, left), showing regions of the surface where the adsorbate yield is low. Similar "dark" regions of low ion yield also appear in gated-substrate images (top, left). Variations in species abundance and field-induced binding must be considered in studies of helium adsorption, both on the surface and in the lattice.

---

* J. A. Panitz, J. Vac. Sci. Technol. 12, 210 (1975).

$p = 3.1 \times 10^{-10}$ Torr

100 Events/ 300 sec

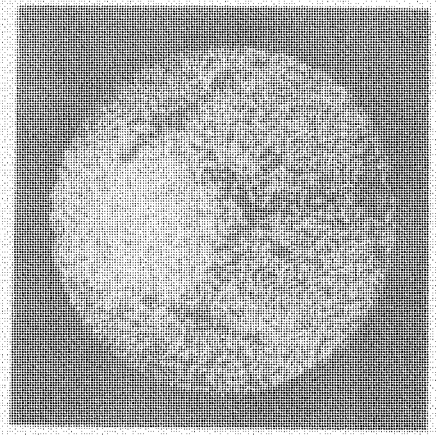

$p = 7.2 \times 10^{-10}$ Torr Ne

150 Events/ 375 sec

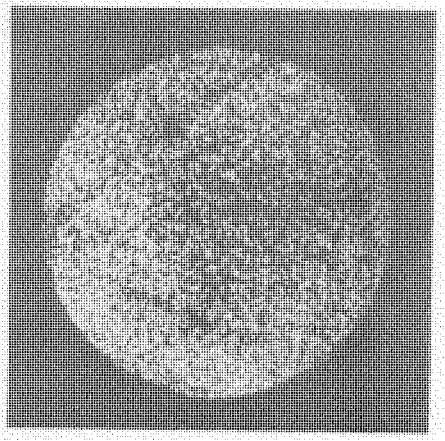

FIELD DESORPTION OF HELIUM AND NEON FROM (111) TUNGSTEN AT 78^{0}K

81574/81674

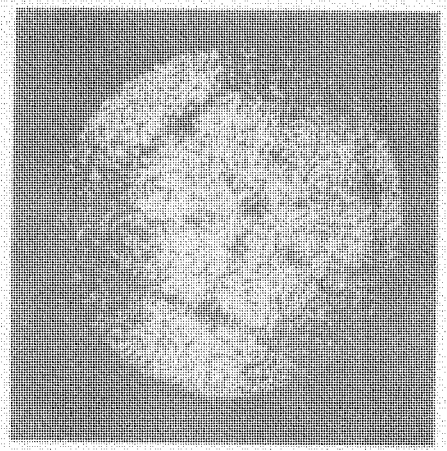

150 Events/ 450 sec

$p = 4.3 \times 10^{-10}$ Torr He

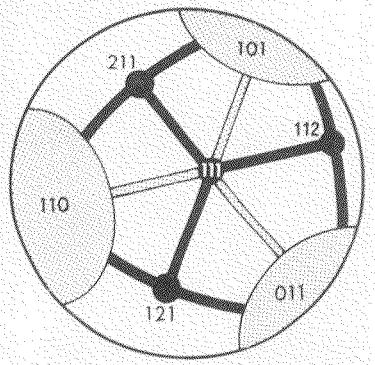

■ SMALL ABUNDANCE OF ANY SPECIES

$(W^{3+} / He^{+}) >> 1.0$ (WHe^{3+} ABUNDANT)

GLOSSARY OF TERMS

Field-ionization: The quantum-mechanical process by which a high electric field (> 10V/nm) increases the probability of electron-tunneling from a neutral gas species into a nearby (40 nm) metal surface.

Field-ion Image: The approximately radial projection of field-ionized gas atoms (formed above a metal surface) to a fluorescent screen producing a pattern of variations in ionization probability, reflecting the position of individual atoms on the metal surface: above protruding (edge, or "kink-site") atoms the electric field will be large, producing a high ion current; above closely spaced atoms the field will be low producing a small ion current.

Field-desorption: The high-field process by which a substrate or adsorbed species is removed from the surface as a positive ion. The process can be interpreted as thermal activation over a field-reduced energy barrier.

Field-evaporation: A particular type of "field-desorption" referring specifically to the field-enhanced removal of substrate (lattice) atoms only.

Field-Adsorption: A Field-induced dipole-dipole bond between a field-polarized substrate and adsorbate atom.

The Atom-Probe Field Ion Microscope*†

ERWIN W. MÜLLER, JOHN A. PANITZ, AND S. BROOKS MCLANE
Department of Physics, The Pennsylvania State University, University Park, Pennsylvania 16802
(Received 1 September 1967)

A serious limitation of the field ion microscope has been its inability to identify the chemical nature of the individually imaged atoms. The newly conceived atom-probe FIM is a combination probe-hole FIM and mass spectrometer having single particle sensitivity. During observation, the observer selects an atomic site of interest by placing it over a probe hole in the image screen. Pulsed field evaporation sends the chosen particle through the hole and into the spectrometer section. Preliminary results show that field evaporation of tungsten under poor vacuum conditions occurs as triply or quadruply charged WO, WN, WO_2, and WN_2 ions, while under better conditions doubly and possibly triply charged tungsten can be observed. Mo-Re alloys always produced doubly charged molybdenum and rhenium ions when examined in the atom-probe. Wide applications for the study of short range order in alloys, the chemical nature of precipitates and impurity atoms, and information regarding the imaging properties of various atom species, of both the substrate and adsorbed material, are foreseen.

I. INTRODUCTION

THE field ion microscope[1,2] provides an intimate view of the location of individual atoms on a metal surface. However, its inability to discriminate between different atomic species has been a serious shortcoming. While it is very certain that only one kind of atom is present on pure W, Ir, or Pt surfaces characterized by a highly perfect FIM pattern, it is not possible to unambiguously identify the different atomic species in the usually less regular FIM patterns which are obtained from alloys, crystals containing impurities, or adsorbates at the surface.

It is quite clear that a basic advance in field ion microscopy would be achieved with the identification of the atomic species associated with individual image dots. This difficult task now appears possible with a combination field ion microscope and mass spectrometer having single particle detection capability. Such a device may be called an atom-probe FIM in analogy with the well known electron microprobe developed by Castaing.[3] The latter instrument, a combination electron microscope and x-ray analyzer, can investigate the constituents of a small section of specimen which, although typically of the order of 1 μ in size, still contains some 10^{11} atoms. In the scanning electron microscope developed by Crewe[4] a very crude form of analysis is believed to be possible from the specific energy losses, but the number of atoms involved is still of the order of 10^5.

In the atom-probe FIM we wish to determine the nature of one single atom seen on a metal surface and selected from neighboring atoms at the discretion of the observer.

II. PRINCIPLE

The atom-probe consists of a field ion microscope modified so that the imaged atom chosen for analysis can be positioned over a probe hole in its fluorescent screen. This hole provides an entrance into the analyzer which in the present design is a time-of-flight spectrometer incorporating a detector having single particle sensitivity. After properly positioning the desired atom and pumping the imaging gas from the microscope, a high voltage pulse applied to the tip desorbs the atomic species which then travels through the probe hole. This pulse also initiates the horizontal sweep of an oscilloscope. When the ion reaches the detector a voltage pulse is fed to the oscilloscope, and thus the time-of-flight of the ion is determined. From these data its mass-to-charge ratio can be calculated since the ion acquires essentially its final velocity within a few tip radii, and since the potential difference through which it travels can be accurately measured. The desorption voltage V is, approximately, this potential difference, which is just the sum of the dc imaging voltage and the maximum pulse voltage, since the rise time of the pulse is negligible compared to the time of flight of the ion, and since the pulse amplitude is much less than the imaging voltage.

The mass-to-charge ratio of the detected ion is calculated from the relations

$$\tfrac{1}{2}mv^2=neV \quad \text{and} \quad v=d/t,$$

where m is the mass of the ion, v is its velocity, ne is its charge, d is the distance between tip and detector, and t is the observed time of flight. One finds, for a tip-to-detector distance of 82 cm, that

$$m/n=0.288Vt^2, \tag{1}$$

where m is measured in amu, V is in kilovolts, and t is in microseconds.

* Supported by the National Science Foundation.

† This paper was presented previously at the 14th Field Emission Symposium at the MBS, Washington, D. C. (June 1967).

[1] E. W. Müller, "Field Ionization and Field Ion Microscopy," in *Advances in Electronics and Electron Physics* (Academic Press Inc., New York, 1960), Vol. 13, pp. 83–179.

[2] E. W. Müller, Science **149**, 591 (1965).

[3] R. Castaing, "Electron Probe Microanalysis," in *Advances in Electronics and Electron Physics* (Academic Press Inc., New York, 1960), Vol. 13, pp. 317–384.

[4] A. V. Crewe, Science **154**, 729 (1966).

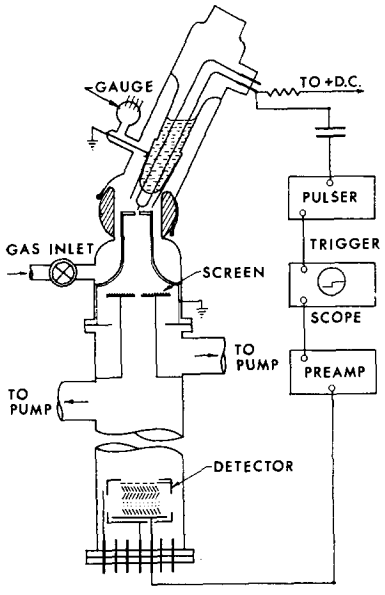

FIG. 1. The atom-probe field ion microscope.

Although our prototype instrument incorporates a time-of-flight analyzer, we are considering the use of other analyzers, including a magnetic sector field with associated multiple detectors. Such a device should permit rapid, consecutive identification of many image spots since the removal of the imaging gas during the desorption process would be unnecessary.

III. A PROTOTYPE ATOM-PROBE FIM

Figure 1 shows a composite view of the atom-probe. During operation the specimen to be examined is mounted on the base of a cold finger and surrounded by an aluminum cone held at ground potential. The cold finger is inserted into the upper portion of the microscope so that the specimen tip is positioned at the center of rotation of the ball joint. When so placed, the tip is axially aligned with respect to the holes located in both the aluminum plate and fluorescent screen. The aluminum plate serves to separate the microscope into two sections. The upper, containing the tip, is connected to a supply of helium gas whose flow rate can be accurately adjusted by means of a variable leak valve. The lower portion containing the fluorescent screen is connected to a liquid nitrogen trapped, 5 cm, oil diffusion pump. During imaging of the specimen, the lower portion of the microscope body is pumped while helium is admitted into the upper portion. This dynamic gas supply system[5] insures that a pressure of about 1 μ is maintained in the immediate vicinity of the tip, while a considerably lower pressure is obtained in the region of the screen.

The time-of-flight tube containing the particle detector and located directly below the fluorescent screen is continuously pumped by a separate, trapped, 5 cm, oil diffusion pump. With the hole size of 1 mm chosen for the fluorescent screen, the vacuum in the vicinity of the multiplier can be maintained, during imaging, at better than 5×10^{-5} Torr. Before actual pulse evaporation the gas supply is shut off and the helium used for imaging is pumped from the microscope ensuring that at a pressure below 10^{-6} Torr an adequate mean free path is obtained.

The evaporation pulse for the atom-probe is taken from a Huggins laboratory pulse generator, model 961-E, having an adjustable pulse amplitude of 0 to 3 kV, a pulse width of 2 nsec, and a rise time and fall time of 0.5 nsec. Manually-triggered single pulses are used in the experiments. The pulse width, rise time, and fall time were confirmed under actual operating conditions by the use of a Tektronix type 519 oscilloscope.

The output of the pulse generator is carried to the microscope head by a 50 Ω coaxial cable terminated by a 50 Ω resistor and coupled to the high voltage leads through a 500 pF, 30 kV capacitor. No attempt was made to clean up reflected secondary pulses as their amplitude is negligible within a period of 100 nsec, which corresponds to less than one mass unit within the voltages likely to be used during normal operation.

The particle detector used is an electron multiplier of the "venetian blind" type, assembled in our Laboratory from 12 dynodes and one anode supplied by EMI (Electrical and Musical Industries, London, England), and baked before use in an auxiliary vacuum system for one hour at 360°C and 10^{-5} Torr. The Be-Cu dynodes are stacked on three ceramic rods and separated from each other by ceramic spacers. They are maintained at appropriate potentials by a resistor chain. A fine wire mesh placed in front of the first dynode and separared from it electrically by two 2 MΩ carbon resistors provides a means of accelerating the incoming ion slightly before striking the first dynode. An electropolished nickel cap covers the mesh and first two dynodes. It is maintained at the same potential (−3000 V dc) as the wire mesh and serves to discourage field emission from possible sharp edges on those initial dynodes held at large negative dc potentials. The entire multiplier is rigidly mounted on an O-ring flange bolted to the base of the time-of-flight tube. All external electrical connections including the multiplier output are made through ceramic-to-metal seals soldered to the flange.

The output of the particle detector is connected to a transistorized preamplifier with an input resistance greater than 10^8 Ω and an output resistance of less than 500 Ω. The detector-preamp combination provides an over-all current gain of greater than 10^{12}. Tests with a Tektronix type 519 oscilloscope showed that for capacitive coupling the preamplifier has a frequency response in excess of 200 MHz. The 16 nsec rise time of the Tektronix type 551 oscilloscope, used to measure the time of flight, determined the rise time of the pulse; the fall time of 1 msec was determined

[5] B. Waclawski and E. W. Müller, J. Appl. Phys. 32, 1472 (1961).

by the detector-preamplifier combination. However, this did not limit the usefulness of the combination in resolving adjacent masses, as a staircase wave shape resulted when two or more particles reached the detector during a single sweep. The resolution of the present equipment is about 1 to 2 atomic mass units, entirely sufficient for our preliminary investigations.

At the maximum current sensitivity of the preamplifier-oscilloscope combination, some 5 pA/cm, no dark current noise was perceptible from the detector. However, on slow sweeps a few random events (of the order of one per second) could be detected, and when small amounts of helium were admitted to weakly image the specimen, helium ion pulses were observed in the expected numbers. Using the normal single sweep of 10 μsec which covers all masses of possible interest, and even with only a modest background vacuum of 10^{-6} Torr, a noise signal that could be mistaken for a desorbed ion was never encountered.

Figure 2(a) shows an example of the oscilloscope pattern obtained from the atom-probe examination of tungsten for two different tip voltages. As can be seen, the rise time of the pulse is quite short, but since the sweep is 1 μsec/cm, the decay time of 1 msec produces a horizontal line. The amplitude of the initial transient could be decreased by more thorough shielding, but was ignored since it did not saturate the preamplifier. The initial oscillations were damped in a time shorter than required for the transit of any possible species appearing on the surface of the specimen and were, therefore, also ignored.

IV. EXPERIMENTAL RESULTS

Using Eq. (1) we find for the upper trace in Fig. 2(a) $m/n=71$, and for the lower trace (from left to right) $m/n=53.6$, and $m/n=71.2$. Because of the relatively poor vacuum conditions maintained at the tip (due to the presence of the greased ball joint and an insufficient path for evacuation), we believe ourselves justified in identifying these species as the tungsten-oxygen complexes $^{182}W^{16}O_2^{+++}$ ($m/n=71.3$) and $^{184}W^{16}O_2^{++++}$ ($m/n=54.0$). Both have been observed previously by other experimenters engaged in more conventional mass spectrometry of oxidized tungsten at elevated temperatures using a field ionization emitter.[6] However, in view of the well known occurrence of nitrogen etch[7] in insufficiently evacuated field ion microscopes, the two species observed may also represent three and four-fold charged ions of $^{186}W^{14}N_2$ molecules, and the ion with $m/n=71.2$, $^{182}W^{14}N_2^{+++}$.

Because of the preliminary design of the present system it was impossible to photograph the screen both before and after evaporation to obtain a precise indication of the location of the species being examined. In the lower trace, clearly, the probe hole was situated so as to allow two neighboring species to be detected. This condition is quite reproducible and, in fact, was observed at other tip voltages, as well as for other tips of the same material imaged in an identical manner.

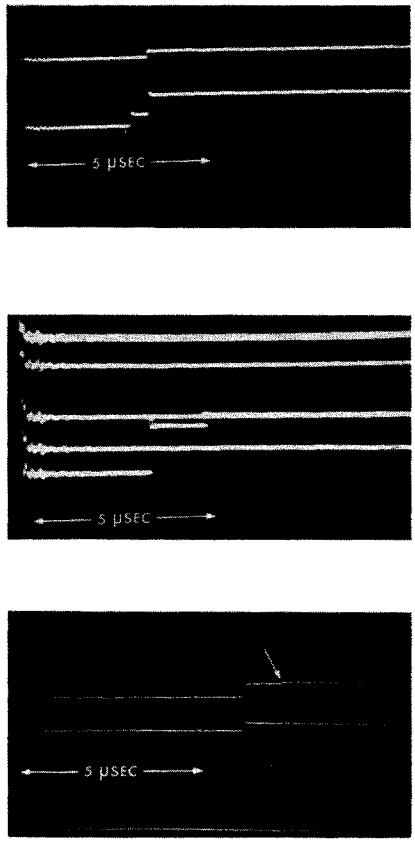

FIG. 2 (a) Atom-probe examination of tungsten; upper trace—25 kV dc +2.4 kV pulse; $m/n=71$ ($t=3.0$ μsec). Lower trace—25 kV dc+2.5 kV pulse;(from left to right) $m/n=53.6$ ($t=2.6$ μsec), $m/n=71.2$ ($t=3.0$ μsec). (b) Atom-probe examination of a rhenium molybdenum alloy; 15.5 kV dc+1 kV pulse; (from left to right) $m/n=48$ ($t=3.2$ μsec), $m/n=93$ ($t=4.4$ μsec). (c) Atom-probe examination of tungsten; Upper trace—9 kV dc+0.2 kV pulse; (from left to right) $m/n=66$ ($t=5.0$ μsec), $m/n=91$ ($t=5.8$ μsec). Lower trace—9 kV dc +0.2 kV pulse; $m/n=66$ ($t=5.0$ μsec).

Figure 2(b) shows the result of using the atom-probe to examine a rhenium-molybdenum alloy, field evaporated at 78°K. Here, once again, is one of a series of photographs in which two atomic species were detected. In this photograph, the smaller ratio (corresponding to the shorter time) is $m/n=48$, while the larger ratio is $m/n=93$. These correspond, respectively, to $^{96}Mo^{++}$ and Re^{++}. The mass-to-charge determination is accurate to about ± 1 amu.

Figure 2(c) resulted from an examination of tungsten at 21°K. A getter had been installed near the tip to improve the vacuum conditions during desorption. Both traces resulted from an imaging voltage of 9 kV, and a pulse voltage of 200 V. Using Eq. (1) one obtains for the upper trace (from left to right) $m/n=66$ and $m/n=91$. For the

[6] R. Vanselow and W. A. Schmidt, 12th Field Emission Symposium (The Pennsylvania State Univ., 1965).

[7] J. F. Mulson and E. W. Müller, J. Chem. Phys. 38, 2615 (1963).

lower trace $m/n=66$. We believe $m/n=91$ corresponds to $^{182}W^{+++}$ while $m/n=66$ corresponds, most probably, to $^{182}W^{16}O^{+++}$ or $^{184}W^{14}N^{+++}$. Of some thirty traces resulting from four specimen tips, W^{++} was observed on only three occasions. The majority of the remaining traces were the tungsten-oxygen or tungsten-nitrogen complexes described earlier. A mass-to-charge ratio between 62.9 and 64.6 was obtained in five cases. This might correspond to $^{186}W^{+++}$ ($m/n=62$), or perhaps to $^{182}W^{14}N^{+++}$ or $^{182}W^{16}O^{+++}$ with $m/n=65.3$ or 66, respectively. Because of the remaining uncertainty of interpretations, no definite conclusions could be drawn, at this time, about the relative abundances of W^{++} and W^{+++}.

V. DISCUSSION

The results obtained to date with the prototype atom-probe, although limited in scope, are highly successful in that they show the feasibility of this most sensitive mass spectrometer, as well as provide a basis on which to design a more sophisticated instrument. Certainly, our experience has shown that it must include such necessary refinements as an adjustable probe hole, and a means to accurately photograph the image both before and after pulse evaporation. In addition, it seems necessary to employ a grease-free, all metal, ultrahigh vacuum system so as to minimize possible tip contamination. These considerations have been incorporated into an instrument which is now being constructed in our Laboratory.

What can be expected of the new technique? It should now be possible to settle the controversy among field ion microscopists concerning the nature of the bright spots obtained by adsorption of oxygen, nitrogen, and carbon monoxide, which have been suggested as representing either adsorbates[8] or tungsten atoms displaced by the corrosion process.[9,10] We will be able to identify the chemical complexes involved in water-etch[7] and oxygen corrosion,[9] as well as the products of reactions initiated under the extreme electric fields encountered at the surface of a specimen. We believe we now have a powerful tool for alloy research since we can determine, quite easily, short range order, discrete visibility of atomic species,[11] and other related items of interest. Finally, the chemical nature of interstitials, segregations, and precipitates will be open to direct experimental observation and analysis.

[8] G. Ehrlich, Discussions Faraday Soc. **41**, 55 (1966).
[9] E. W. Müller, "FIM Studies of Surface Corrosion of Interstitials, Vacancies and α-Irradiation Damage by Controlled Field Evaporation of Atomic Layers," in *Structure and Properties of Thin Films*, C. A. Neugebauer, J. B. Newkirk, D. A. Vermilyea, Eds. (John Wiley & Sons, Inc., New York, 1959), p. 476.
[10] A. A. Holscher and W. M. H. Sachtler, Discussions Faraday Soc. **41**, 29, 54, 70 (1966).
[11] T. T. Tsong and E. W. Müller, Appl. Phys. Letters **9**, 7 (1966).

THE REVIEW OF SCIENTIFIC INSTRUMENTS VOLUME 39, NUMBER 1 JANUARY 1968

Recording Fabry-Perot Interferometer

H. G. KUHN, E. L. LEWIS, D. N. STACEY, AND J. M. VAUGHAN*
Clarendon Laboratory, Oxford, England
(Received 26 July 1967; and in final form, 19 September 1967)

A recording interferometer is described in which a direct plot of spectral intensity against wavenumber is obtained without the use of a time base. When used as a double recorder, the instrument records two spectral profiles simultaneously. In this form, the recorder is particularly suited to the comparison of spectral profiles and the measurement of small line shifts.

INTRODUCTION

PHOTOELECTRIC recording is now a well established technique of interference spectroscopy. In the most widely used method, [1,2] the optical path in a Fabry-Perot etalon is varied by changing the pressure of the gas between the plates, and the intensity at the center of the fringe pattern is plotted against time by means of a chart recorder. To obtain a linear wavenumber scale, it is necessary to vary the pressure at a constant rate. The difficulties involved in controlling the pressure variation to the required degree of accuracy led to the development of the direct-recording interferometers now in use at the Clarendon Laboratory. These avoid the necessity for a time base, since the intensity in the center of the fringe pattern is plotted directly against the pressure in the etalon box.

The recorders have now been in use for several years in investigations requiring the detailed analysis of spectral

* Present address: Palmer Physical Laboratory, Princeton University, Princeton, N. J.
[1] P. Jacquinot and Ch. Dufour, J. Rech. Centre Natl. Rech. Sci., Lab. Bellevue (Paris) **6**, 91 (1949).
[2] P. Jacquinot, Rept. Progr. Phys. **23**, 267 (1960).

The crystallographic distribution of field-desorbed species*

J. A. Panitz

Sandia Laboratories, Albuquerque, New Mexico 87115
(Received 13 August 1973)

The complete crystallographic distribution of field-evaporated W^{3+} and W^{4+} as well as field-desorbed hydrogen has been observed by using a new technique called field desorption spectrometry. The distributions are obtained during a single evaporation event in a modified field-ion microscope by recording the desorption image displayed on a spherical CEMA detector time gated with the arrival of an ion species of preselected mass-to-charge ratio. Preliminary observations show no unique crystallographic origin for W^{3+} or W^{4+} at 78 or 27 K during field evaporation in vacuum or imaging gas. Hydrogen appears to originate at random insterstitial locations at the surface and is not uniquely associated with the protruding atoms imaged in a conventional ion micrograph. The general lack of a one-to-one correspondence between gated desorption and ion micrograph images suggests that using the atom probe to identify individual preselected ion micrograph image spots may be much more difficult than originally anticipated.

INTRODUCTION

The field-ion microscope[1] provides a simple but elegant means for observing a metal surface in atomic resolution. With the introduction of the atom probe[2] in 1967, the identity of individual surface species could be determined, providing a surface analytical device with single-atom resolution. Recently, a variation of the atom probe[3] has extended its capability to include single-atom identification at several different crystallographic locations during a single evaporation event in addition to permitting all imaged surface species to be identified at one time. In this paper we present a logical extension of this latter technique, yet one which departs completely from atom probe philosophy. Rather than attempt to determine the identity of a surface species producing a preselected ion-image spot, we wish to determine the complete crystallographic distribution of a surface species of preselected mass-to-charge ratio. The significant advantage of this approach is that one obtains the complete surface distribution of a given species during a single evaporation event and thereby avoids the surface altering and tedious procedure inherent in any statistically significant crystallographic distribution determination using the atom probe. We call this new technique field desorption spectrometry (FDS) and use it here to provide the first comprehensive crystallographic distribution data for the species present on the surface of clean tungsten.

THEORY

Surface species, field evaporated from the specimen as positive ions by a high-voltage pulse, enter the drift region of a time-of-flight spectrometer with energy

$$\tfrac{1}{2}mv^2 = qV_A = neV_A, \tag{1}$$

where m is the mass of any single ion, v is its velocity, q is its charge, e is the electronic charge, and V_A is a positive bias applied to the specimen.

After traveling a time T in the drift region of length d, given by

$$T = d/v, \tag{2}$$

the ions strike a curved Chevron CEMA detector,[4] providing a visible desorption image on its phosphor screen that can be photographically recorded. The travel time of a given ion species is obtained by combining Eqs. (1) and (2) to give

$$T = d[(m/n)(0.193V_A)^{-1}]^{\frac{1}{2}} \tag{3}$$

where T is in μsec, d is in meters, m/n is in amu, and V_A is in kV. Now suppose that instead of operating the CEMA continuously, it is turned on for a short time

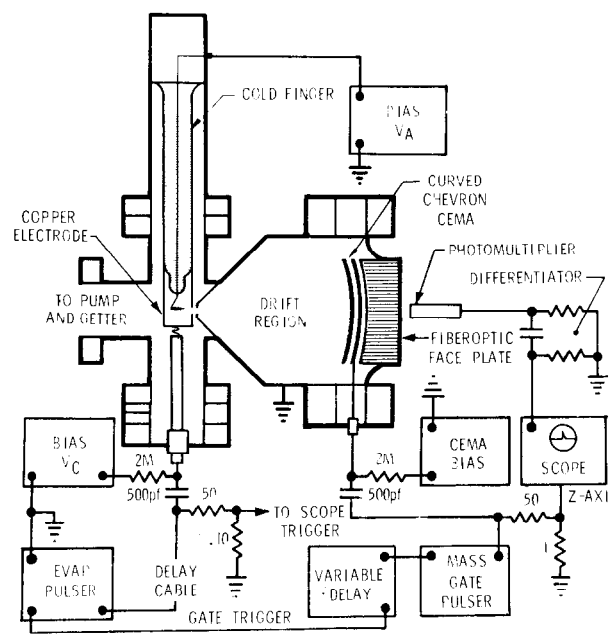

FIG. 1. Field desorption spectrometer. Desorbed surface species are detected by a time-gated curved Chevron CEMA detector so that only ions having a preselected mass-to-charge ratio will be displayed on its phosphor screen. This permits the complete crystallographic dependence of the given species to be recorded during a single evaporation event by placing photographic film (Polaroid Type 57) in contact with the CEMA's fiber-optic face plate. The delay cable from the evaporation pulser compensates for the inherent delay in the variable and mass gate pulsers.

coincidentally with the arrival of a preselected species of interest by applying a gate pulse a time T after the evaporation pulse has reached the specimen. If the duration of the gate pulse is shorter than the travel time between adjacent species, only that surface species having the unique travel time T will be detected and its complete crystallographic distribution displayed. Since individual ion impacts are resolved and recorded photographically, the number of recorded spots gives the absolute abundance of the detected species.[5]

APPARATUS

The apparatus is shown schematically in Fig. 1 and is identical to that described previously[3] except for the addition of the gating circuitry. During continuous operation of the CEMA (mass gate operative but not connected), the photomultiplier records the arrival of all ion species, and the resulting differentiated signal is displayed on an oscilloscope whose sweep is initiated by the evaporation pulse. A sample of this pulse is also displayed to provide a zero-time "fiducial" mark, and a sample of the gate pulse is used to modulate the oscilloscope sweep intensity so that the position of the mass gate relative to the ion peaks can be conveniently determined.

After selecting a species for investigation, the delay of the mass gate relative to the evaporation pulse is adjusted with the variable-delay generator until the intensified portion of the sweep coincides with the selected ion peak. The CEMA is then operated with the mass gate connected and the photomultiplier used to verify that the gated detector displays only the selected species. The optical coupling between the fiberoptics and the photomultiplier effectively isolates the sensitive photomultiplier circuitry from the fast high-voltage gate pulse.

FIG. 2. Helium ion image of the tungsten surface used in this study at 27 K and 6×10^{-7} Torr helium.

FIG. 3. Gated desorption image of W^{3+} at 78 K and 4×10^{-9} Torr during "gentle" evaporation. The complete crystallographic distribution of this species is displayed. Only the 110 region can be easily identified. Ion energy, 5.58 kV; $V_C=-5$ kV; $V_p=-1.5$ kV.

DETECTOR

During continuous operation, the curved CEMA is operated with 1 kV across each plate and 7 kV between the second plate and the screen. The front surface of the CEMA, which defines the end of the ion drift region, is usually held at ground potential.

To achieve gated operation, a positive pulse of 800 V is applied to the CEMA surface closest to the screen after reducing its dc potential to 1200 V.[6] Without applying the gate pulse, the CEMA gain is effectively zero, and no random noise images can be detected on Polaroid Type 57 film after a 30-sec exposure. Because only the ion species selected for examination is time correlated with the application of the narrow gate pulse, the signal-to-noise ratio of the detector is essentially infinite. This can be confirmed by moving the gate pulse in time to a position at which no ions were detected during nongated operation of the CEMA and exposing Type 57 film.

FIG. 4. Gated desorption image of W^{3+} at 78 K and 4×10^{-9} Torr during "severe" evaporation. The crystallographic distribution is essentially uniform. Ion energy, 5.58 kV; $V_C=-5$ kV; $V_p=-2.0$ kV.

In order to optimize both viewing and photographing of the gated image, a long-decay-time phosphor is desirable, but, since the arrival of the ions at the CEMA must be accurately determined by the photomultiplier, a short rise time is essential. These two diverse conditions are satisfied by settling equal parts of P1 and P47 phosphors on the fiberoptics viewing screen. The P1 phosphor provides a bright image for visual observation and photography, and the P47, matching the spectral response of the photomultiplier, provides the fast rise time which is required.

RESULTS AND CONCLUSIONS

Figure 2 shows a conventional helium ion image at 27 K of the tungsten surface used in this study. Since a desorption micrograph is always sharper than the corresponding ion micrograph, even at elevated temperatures,[7] much of our work has been done at 78 K.

Figure 3 is an example of mass gating for the dominant ion species W^{3+} and applying a desorption pulse to cause "gentle" field evaporation of the surface. Two features of this gated desorption micrograph are immediately obvious. First, W^{3+} does not appear to originate from specific crystallographic locations but appears to come from all areas of the surface with equal probability. Second, and perhaps more striking, is the general lack of a recognizable ion micrograph pattern. That is, there is not a unique one-to-one correspondence between the surface species imaged in the conventional ion micrograph and those recorded as a result of field evaporation. This does not appear to be due to CEMA characteristics as previously supposed[7] since there is obvious net plane symmetry in the 110 region that can be directly correlated with edge atoms imaged in the conventional ion micrograph. Rather, the disorder appears to be due to a statistical feature of the evaporation process, as well as local field variations (caused by local variations of the specimen's average radius of curvature) which cause locally different evaporation rates.[8] This is emphasized in Fig. 4, where W^{3+} was once again examined but at a much higher evaporation rate. The imaged area has in general begun to "fill in" while still preserving the identity of the 110 region. Since this region has the highest evaporation field of those imaged, the "filling in" of the micrograph is probably due to much more rapid evaporation in all other areas, which results in continual local removal of atoms from the specimen throughout a depth of perhaps several atomic layers.

Of particular interest are those atoms which appear to have field evaporated from the central area of the 110 plane or from the surrounding ledges, atoms which are

FIG. 5. Gated desorption image of W^{4+} at 78 K and 4×10^{-9} Torr. Ion energy, 2.5 V; $V_C=-6.25$ kV; $V_p=-1.3$ kV. The evaporation rate, as determined by monitoring W^{3+}, was severe since only under such conditions is the appearance of W^{4+} noticeable. The specimen is not the same one used to obtain Figs. 2–4 and 6.

not imaged in a conventional ion micrograph[9] and represent a very real manifestation of the statistical nature of the evaporation process. It is interesting to notice the converse at gentle evaporation rates (Fig. 3) where the statistical nature of the process is still evident. There, conventionally imaged atoms (edge atoms of the 110 plane) do not all field evaporate, as might be expected from *a priori* considerations.

As a result of the apparent statistical nature of the evaporation process, the ultimate aim of atom probe microscopy, "to determine the nature of one single atom seen on a metal surface and selected from neighboring atoms at the discretion of the observer,"[10] may be extremely difficult to achieve. This does not, however, detract from the more usual and practical use of the technique as an ultimate microanalytical capability for identifying the species present in a *small region* of the surface.

It is important to distinguish the lack of correlation between ion and gated desorption micrographs due to the statistical nature of the evaporation process or to local variations in evaporation rate from the lack of correlation due to a trajectory difference between the ionized imaging gas atom and the corresponding field-evaporated surface species.[11] In theory, one can compensate for this latter "aiming effect" in the atom probe by shifting the probe hole slightly away from the selected ion micrograph image spot[12] until a signal is recorded at the detector. In practice, however, the statistical nature of the evaporation process interferes since the detected signal may either represent the species originally intended for examination or a completely different species not originally imaged. Only by using a large probe hole several ion image spots in diameter to assure the detection of *something* can one eliminate this problem, but in doing so spatial resolution on the surface must be sacrificed.

If the instrument is gated for the less abundant species W^{4+} ($W^{4+} < 0.1W^{3+}$), one obtains the micrograph shown in Fig. 5. The most obvious feature of the W^{4+} micrograph when compared to those of W^{3+} is the lack of symmetry or indication of net plane structure in the 110 region. It is tempting to suggest that the production of W^{4+} is related, statistically, to W^{3+} production and one could produce a W^{4+} pattern by picking at random every tenth atom from a W^{3+} micrograph obtained during severe evaporation. In any event W^{4+}, which does not appear unless the evaporation rate is very large,[13] does not exhibit a strong crystallographic dependence but appears to be produced with essentially equal probability over the entire imaged surface.

Figure 6 is the result of gating for hydrogen adsorbed on the surface from residual hydrogen in the vacuum system. Since our resolution is not presently sufficient to separate mass 1 and 3, Fig. 4 may contain the desorption images of H_1^+, H_2^+, and H_3^+. Of particular interest is the lack of recognizable surface features. Since hydrogen was desorbed from the surface, the randomness of its pattern implies that it is adsorbed at interstitial locations on the surface and does not preferentially associate with the protruding atoms imaged in a conventional ion micrograph. There is a suggestion from Fig. 5 when compared with the ion micrograph image of Fig. 3 (and enforced by repeated desorption observations) that the 110 region contains less adsorbed hydrogen than the regions closer to the tip shank. This may be reasonable since migration from the shank would be expected to at least partially replenish the surface coverage between evaporation pulses.

FIG. 6. Gated desorption image of residual hydrogen field desorbed from the tungsten emitter shown in Fig. 1 at 78 K and 6×10^{-9} Torr. The lack of symmetry, particularly in the 110 region, suggests that hydrogen is field desorbed from random interstitial locations on the surface. Ion energy, 4.0 kV; $V_C = -5.5$ kV; $V_p = -1.5$ kV.

ACKNOWLEDGMENTS

The author wishes to thank J. Abraham of the Bendix Corp. who manufactured the curved CEMA plates in an elegantly simple manner, V. Nogle for his technical assistance, and R. Snidow and F. Tenant for their cooperation and glass-working expertise.

*Supported by the U. S. Atomic Energy Commission.

[1] E. W. Müller and T. T. Tsong, in *Field Ion Microscopy, Principles and Applications* (Elsevier, New York, 1969).

[2] E. W. Müller and J. A. Panitz, 14th Field Emission Symposium, National Bureau of Standards, Washington, D. C., (unpublished).

[3] J. A. Panitz, Rev. Sci. Instrum. **44**, 1034 (1973).

[4] Manufactured by The Bendix Corp., Electro-Optics Division, Galileo Park, Sturbridge, Mass. The specimen is placed at the

center of curvature of the CEMA to ensure identical travel times for all ion species.

[5]The absolute abundance of the detected species on the surface *prior* to field evaporation can be determined from these data only if the entire surface layer of atoms has been removed and if the active area of the CEMA is sufficiently large to assure detection of essentially all ions striking it.

[6]The width of the gate pulse essentially determines the mass resolution, since it provides a "time window" during which the CEMA has gain. At its maximum amplitude of 800 V the gate pulse is 10 nsec wide, and its width increases to 30 nsec at 200 V. At this point the total potential (dc bias +pulse amplitude) is 1000 V, and the resulting CEMA gain is insufficient to detect desorbed species.

[7]A desorption microscope using a single channel plate and external image intensifier was described by R. J. Walko and E. W. Müller, Phys. Status Solidi A **9**, K9 (1972). Mass analysis of the detected species was not possible.

[8]An alternate explanation is that a surface species, immediately prior to removal from the surface as a positive ion, exists in a metastable state whose surface location does not coincide with the species' original surface position. Subsequent removal from this new surface position would lead to a detected image lacking correspondence with a conventional ion image. However, this mechanism does not appear to be too probable in view of the 110 region symmetry unless its importance is dependent on specific crystallographic location.

[9]Another possibility is that such images represent conventionally imaged surface atoms whose trajections during field evaporation are significantly but randomly altered from those of neighboring species. Since the probability of appearance of the "misplaced" atoms seems to increase directly with the severity of the evaporation event, it is usually desirable to minimize the evaporation rate consistent with the ability to remove species of interest.

[10]E. W. Müller, J. A. Panitz, and S. B. McLane, Rev. Sci. Instrum. **39**, 83 (1968).

[11]E. W. Müller, 15th Field Emission Symposium, Bonn, Germany 1968 (unpublished); J. A. Panitz, Ph.D. dissertation, The Pennsylvania State University, 1969.

[12]E. W. Müller, Ber. Bunsenges. **75**, 979 (1971).

[13]It is not obvious whether the production of W^{4+} is due to a large evaporation rate or to the correspondingly large evaporation field. That is, it is difficult to determine if the production mechanism is rate or field-dependent.

The 10 cm Atom Probe*

J. A. Panitz
Sandia Laboratories, Albuquerque, New Mexico 87115
(Received 12 February 1973; and in final form, 16 April 1973)

A novel atom probe is described which can determine the mass-to-charge ratios of all ion species produced during a single desorption event or of individual species at several preselected crystallographic locations during each desorption event. This is accomplished without tip movement in an instrument no larger than a conventional field ion microscope by using a new channel plate photomultiplier detector. Alignment, aiming, and pulse stability problems common to all previous designs have been eliminated. Although the present mass resolution is 4 amu at $m/n = 184/3$, single isotope resolution, if desired, seems possible.

INTRODUCTION

The atom-probe field ion microscope[1–5] is a unique instrument providing the ultimate in micromass analysis of metal surfaces. Unfortunately, the atom-by-atom identification of the surface provided by the device is tedious, particularly in those metallurgical applications requiring composition analysis throughout the bulk of a specimen. Furthermore, most of the instruments discussed in the literature have been large and cumbersome, usually requiring differential pumping of the spectrometer and complicated mechanisms for moving the emitter. As a result, atom-probe investigations have been successfully undertaken by only a few individuals, the device remaining for the most part a highly specialized laboratory instrument. It is the purpose of this paper to describe a new and simple atom-probe which permits rapid, in depth species identification or the more usual atom-by-atom analysis provided by its predecessors. This has been accomplished with an instrument having a volume of less than two liters in which tip movement is unnecessary and the problems of evaporation pulse stability and alignment common to all previous designs have been eliminated. Although the mass-to-charge ratios of desorbed species are still determined by a time-of-flight technique, the drift region has been made an order of magnitude shorter than that of previous instruments. This permits the entire surface of the specimen under investigation to be imaged directly at the detector, and a novel scheme allows for precise species identification at one or several preselected image spots during a single evaporation pulse without the use of a "probe hole."

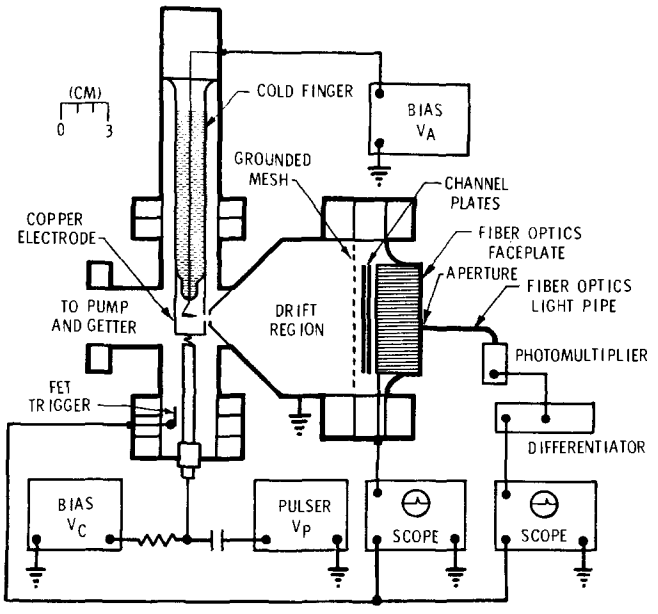

FIG. 1. The atom probe and associated electronic circuitry. Imaging is done at the detector, eliminating the need for a probe hole or a mechanism to move the specimen. The ions produced at the specimen surface are accelerated toward the copper electrode and are decelerated between the copper electrode and the entrance to the drift region. As a result, the ion energy in the drift region is determined only by the bias voltage $+V_A$. The evaporation pulse amplitude and duration are no longer important. By observing the desorption image directly, evaporation rates in vacuum can be precisely controlled, and the aiming problem of previous instruments completely eliminated.

PRINCIPLE OF OPERATION

The new atom-probe as shown in Fig. 1 consists of a field ion microscope with a channel plate electron multiplier assembly replacing the conventional fluorescent screen. A bias voltage $+V_A$ is applied to a stationary tip assembly of conventional design[6] surrounded by a cylindrical electrode held at a potential $-V_C$ sufficient to establish the required imaging field. An aperture in this electrode, opposite the tip, permits ions to travel from the tip into a drift region at ground potential. Between the tip and electrode, ions are accelerated. Between the electrode and the entrance to the drift region, ions are decelerated, so that their kinetic energy within the field-free drift region is determined solely by the magnitude of the positive bias V_A. If a high voltage pulse of sufficient amplitude $-V_P$ is applied to the electrode, an atomic layer is field desorbed from the tip surface,[7] the resulting ions traveling from the tip through the drift region to the first channel plate of the multiplier array. This is in sharp contrast to the operation of previous instruments in which the final kinetic energy of the ions produced by the desorption pulse was determined by a positive bias applied to the tip *and* the magnitude and duration of the desorption pulse itself.

Two modes of detection are possible in the new instrument. If the arrival of the desorbed ions is recorded by connecting the aluminized phosphor of the channel plate array directly to an oscilloscope whose sweep is initiated by the desorption pulse, the travel times of all ions striking the channel plate can be directly measured. Because of the short flight path (~10 cm), essentially all of the specimen is imaged on the channel plate. As a result, all of the ions produced by the desorption event are monitored at one time, permitting a rapid evaluation of species concentration over the entire surface. This is a significant departure from

previous atom-probe philosophy which restricted ion determination to several image spots at best.

The second mode of detection permits atom-by-atom analysis but without the necessity of tip movement and probe hole size considerations common to all previous designs. Imaging gas is introduced at a pressure of 10^{-6} Torr, producing a conventional ion image on the fluorescent screen of the multiplier array. A suitably apertured photomultiplier, external to the vacuum system, is placed over a selected image spot. Its output is differentiated and fed to the input of an oscilloscope whose sweep is triggered by the desorption pulse. Now the travel time of only those ions producing scintillations on the portion of the phosphor screen opposite the apertured photomultiplier will be recorded. If the aperture is equal in size to a single image spot, atom-by-atom analysis is possible; and if several apertured photomultipliers are used, atom-by-atom analysis can be obtained at several different locations. This provides a capability unavailable with all previous instruments in which different crystallographic locations could be examined only by moving the emitter after the evaporation pulse had altered the surface and presumably the location of adsorbates of interest.

Since the ion energy is determined solely by the dc bias applied to the tip and is not affected by the amplitude or duration of the desorption pulse, pulse requirements are noticeably relaxed over previous designs. In fact, the only important requirement is that the pulse is of sufficient amplitude to cause the desorption event and that its risetime is comparable to the uncertainty in the measurement of the ion travel time, thereby eliminating a possible source of timing inaccuracy. If the drift distance is known, the mass-to-charge ratio of detected species can be shown to be simply

$$m/n = Ct^2 \quad C \equiv (0.193/d^2)V_A, \tag{1}$$

where d is measured in m, V_A in kV, t in μsec, and m/n in amu. If V_A is held constant, the travel time for each ion species will be constant and the repetitious m/n calculations of previous atom probes can be eliminated.[8] In practice, V_A is usually fixed at 3 or 4 kV. As the tip radius changes from successive evaporations, the bias voltage V_C is increased to maintain the required imaging field.

The choice of the drift distance, d, is a compromise. It is made as small as possible so that the divergent field-ion image occupies all of the channel plate, while being large enough so that a reasonable bias voltage will provide adequate resolution and ion travel times within the capability of a high speed oscilloscope. Obviously, if the bias voltage is too small, the ion kinetic energy will be small and external magnetic fields will affect the resulting trajectories. Fortunately, for a bias voltage of $V_A \geqq 50$ V, the deflection of an ion at the channel plate due to the earth's magnetic field is negligible.

APPARATUS

The new atom probe is shown in Fig. 2. The specimen to be examined is mounted in the usual fashion at the base of a glass cold finger and surrounded by a copper cylinder to which the negative bias and pulse voltages are applied. When liquid nitrogen is introduced into the cold finger, the copper cylinder contracts and soon reaches 78 K, enhancing image brightness by precooling the imaging gas, thereby improving thermal accommodation with the emitter.[6] Spaced less than 2 mm away is an aperture which defines the entrance to the drift region. The entire assembly as shown is fabricated from inexpensive high vacuum components and is easily pumped to 10^{-9} Torr by a 2 cm trapped oil diffusion pump after a mild bakeout at 200°C for 2 h. A molybdenum getter cooled to 78 K keeps the pressure in the instrument at 3×10^{-9} Torr or lower for a period of several hours without pumping. A microleak valve connected between the system and a 1 liter flask of research grade helium provides the required imaging gas. The use of a channel plate detector permits imaging gas pressures of 10^{-6} Torr or less, eliminating the need for the more elaborate differentially pumped instruments previously described. Although these low pressures insure an adequate mean free path for ions between tip and detector, the imaging gas is often pumped out before field evaporation to eliminate scintillations on the channel plate screen caused by the imaging gas ions.

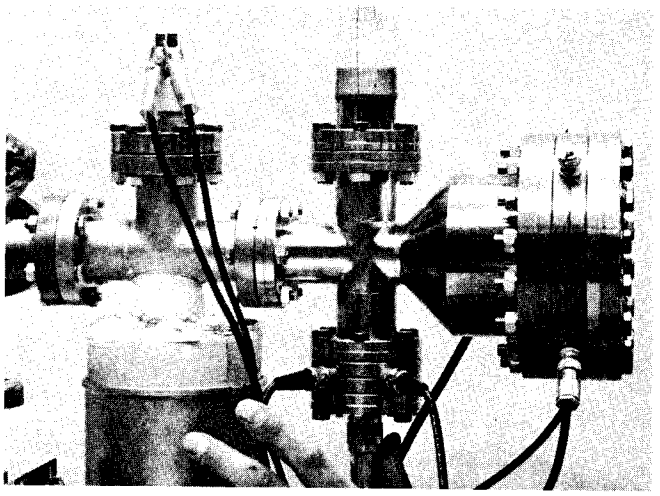

FIG. 2. The atom probe. Photomultiplier and fiber-optics light pipe have been removed for clarity. Note the use of 7 cm vacuum components.

The evaporation pulse is supplied by a pulse generator[9] having a pulse amplitude of 0--20 kV, a pulse width of 200 nsec, and a risetime of less than 5 nsec. The generator is manually triggered and supplies single pulses as required. Since changes in pulse amplitude or duration only affect the evaporation field and not the ion energy in the drift region, carefully terminated pulse lines are no longer a requirement for successful atom probe operation. The elimination of the severe pulse requirements is extremely important since previous work has clearly demonstrated the problems associated with less than ideal evaporation pulse waveshapes.[10] To insure that a minimum and constant delay time is present between triggering the pulse generator and the start of the oscilloscope sweep, the pulse is monitored within 2 cm of the tip by an in-vacuum FET emitter follower[11] which provides the oscilloscope trigger. The bias voltage V_A, which determines the ion kinetic energy, is set by an ultrastable

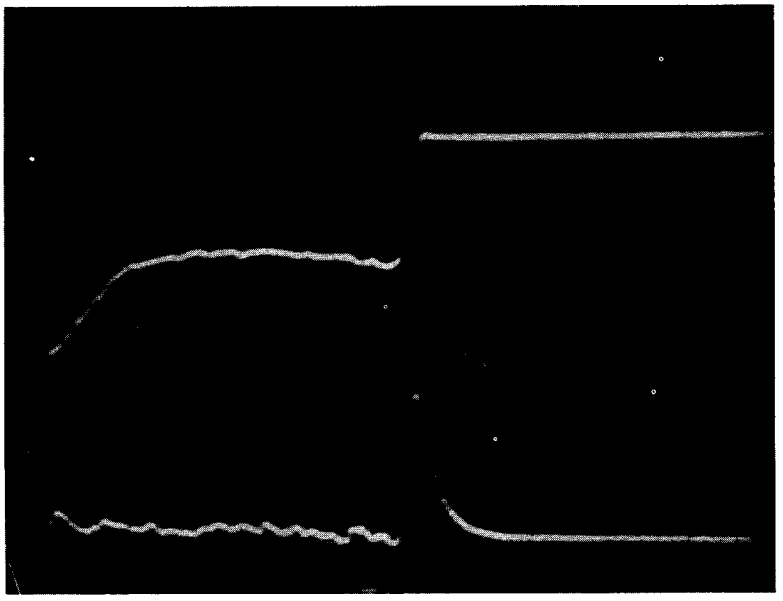

FIG. 3. Undifferentiated output of photomultiplier (upper trace), total decay time of phosphor after increase in intensity due to arrival of final ion species is approximately 1 μsec; differentiated output (lowertrace) 600 nsec/div., $m/n=184/3$ (W^{3+}), $V_A=4$ kV, $V_C=8.75$, $V_P=3$ kV.

dc power supply[12] with 0.001% regulation and a ripple of less than 200 mV.

The detector was assembled from two 75 mm channel plates,[13–15] each cut at a 5° bias and placed in a chevron configuration 3 mm from a deposited P5 phosphor screen. A grounded mesh of 90% transmission was placed in front of the input plate. With 700 V across each plate and 3 kV between the output plate and screen, a gain of 10^5 could be obtained. Ion feedback prevented operation at higher gains, strongly suggesting that one should employ the plate configuration used in a commercially available array having lower noise at higher gains.[16] The grounded mesh at the input permitted the first plate to be held at a large negative voltage so that the screen, at ground potential, could be connected to an oscilloscope. P5 phosphor was chosen because of its rapid risetime and its spectral response which almost exactly matches the RCA 4615 photomultiplier used as a scintillation detector for the single species mode, thereby maximizing over-all sensitivity.

A differentiator at the oscilloscope input extracts the fast risetime phosphor scintillation due to the arrival of desorbed ions from the longer time phosphor decay characteristic (see Fig. 3).

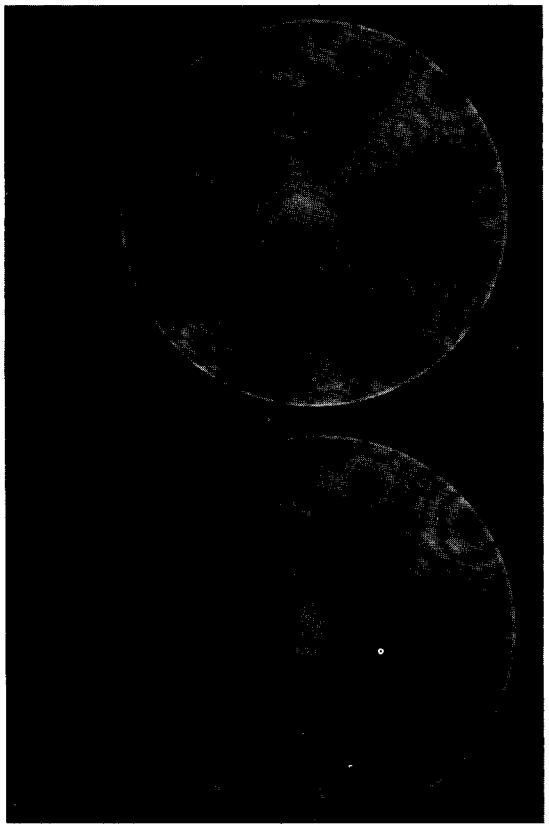

FIG. 4. Ion image at output of channel plate taken through 90% transmitting mesh. Imaging at the detector permits any number of meshes to be inserted in the ion's path since their effect can be visually determined. 6.7×10^{-6} Torr He (78 K), $V_A=9.39$ kV, $V_C=0$ (upper); $V_A=5$ kV, $V_C=4.4$ kV (lower).

AIMING CONSIDERATIONS

Because the detector images the ion pattern, aiming requirements are greatly simplified over previous designs. For example, the displacement of the ion image by a change in the ratio of tip to shield potentials[17] is immediately apparent (see Fig. 4); therefore, the photomultiplier can be positioned over the shifted image spot. It is this capability of selectively positioning over the *shifted* image[18] which makes the electrode configuration of the present design feasible as opposed to an earlier instrument[19] in which a similar pulsing technique could cause ambiguity if preselected sites were to be examined.

In addition, by photographing the image produced by the desorbed ions[20] at the detector (see Fig. 5), a precise position for each desorbed ion can be recorded. Using this information, single preselected atomic sites can finally be examined by placing the photomultiplier at the position of the desired desorbed ion image spot, thereby solving the fundamental aiming problem of all atom probes—the difference in position between the imaging gas and desorbed ion image. In the past, although recognized, this aiming problem has been largely ignored because of the tedious trial and error approach which had to be used to determine the correct probe hole

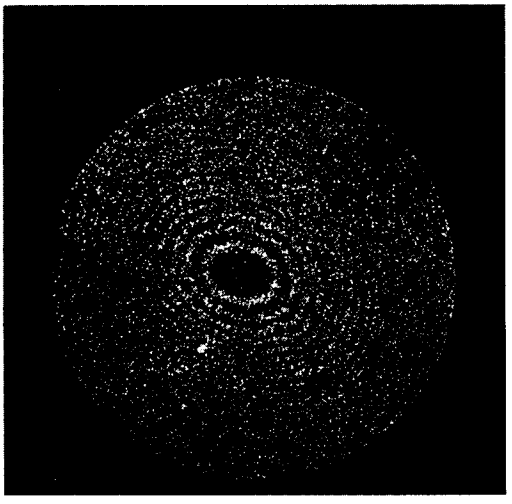

FIG. 5. Desorption image of tungsten at 78 K. $V_A=12$ kV, $V_c=0.5$ kV, $V_P=2$ kV, $P=1.3\times10^{-9}$ Torr. P1+P5 phosphor screen. Image recorded by direct contact of Polaroid (ASA 10 000) film with fiber-optic faceplate of detector (Bendix CEMA, operated at 1700 V) V_P adjusted for gentle evaporation of 110 plane. By visually observing the desorption image, the evaporation rate in vacuum can be accurately selected. Bright area near 110 plane is a detector anomaly.

position.[21] Often, the probe hole was made much larger than the selected image spot to insure that ions were detected and although this corrected for the uncertainty in the desorbed ion's position, it never allowed the atom probe to be used as originally intended—for the detection of a single species preselected at the discretion of the investigator.[2]

CALIBRATION AND RESOLUTION

Calibrating the new atom probe is somewhat easier than calibrating earlier instruments[10] because the ion energy is determined only by an ultrastable dc power supply. As a result, since the drift distance can be accurately measured, the only significant uncertainty can be in the travel time measurement caused by cable, pulser, and sweep delays. This means that Eq. (1) should actually be written as

$$m/n=C(t+\delta)^2, \quad C\equiv(0.193/d^2)V_A, \quad d=0.112\ \text{m}. \quad (2)$$

One simply chooses δ, which could be positive or negative depending on the nature of the delay, so that Eq. (2) predicts the correct m/n value for a known species. Then, provided δ is a constant, Eq. (2) can be used to determine the identity of unknown species. In the present instrument $\delta=+0.091\pm0.005$ μsec and is constant. It should be noted that the drift distance, d, in Eq. (2) is not strictly a constant but depends upon the position of the ion at the channel plate. This is due to the divergent ion trajectories between the tip and the planar grid which defines the end of the drift region. That is, an ion forming an image spot at the extreme edge of the pattern travels a longer distance than the identical ion forming an image near the center of the pattern. By placing a photomultiplier over an image spot at the center of the screen and then over an image spot at its edge, the shift in travel time for a given single species resulting from the different drift distance can be directly measured. In the present instrument this amounts to $\Delta t\cong0.060$ μsec and can accordingly limit resolution when the

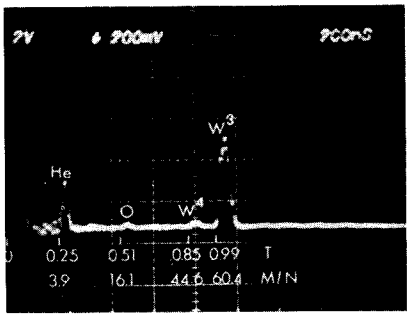

FIG. 6. Direct output from channel plate showing all species present (200 nsec/div.), $V_A=4$ kV, $V_C=8$ kV, $V_P=3$ kV, 6.7×10^{-6} He. Because peak amplitudes change by only 10–15% during successive sweeps, abundance ratios within this uncertainty can be obtained. For example, $W^{4+}/W^{3+}=0.1$.

output of the channel plate is connected directly to an oscilloscope, thereby recording the travel times of all desorbed species (see Fig. 6). Fortunately, the problem can be eliminated by using a hemispherical grid in place of the planar mesh now used. The drift distances would be the same if the tip was placed at the center of curvature of the mesh, although the distance and resulting travel times for ions between the mesh and first channel path would now depend on position. But since the nominal travel time between mesh and channel plate is small compared to the travel time in the drift region, such differences would be unimportant in calculating the mass-to-charge ratio of observed species.

The expected mass resolution *in the single-atom mode* at any image spot can be obtained directly from Eq. (2), noting that the only variable is the travel time t. That is,

$$\frac{\Delta(m/n)}{m/n}=\frac{2\Delta t}{(t+\delta)}.$$

Consider the result obtained by singly differentiating the output of a photomultiplier when examining several image spots of a tungsten emitter by using a large aperture in front of the photomultiplier. One finds from Fig. 7 that for $\Delta t=0.04$ μsec, $t=1.06$ μsec, and $\delta=+0.091$

$$\frac{\Delta(m/n)}{m/n}=0.07$$

or

$$\Delta(m/n)=4\ \text{amu} \quad \text{at} \quad m/n=184/3.$$

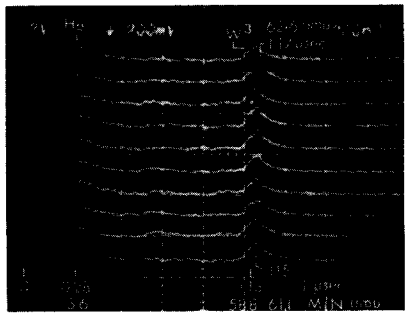

FIG. 7. Differentiated photomultiplier output, 200 nsec/div. Maximum peak separation on successive sweeps due to maximum isotope separation W^{3+} $(m/n=184/3)$. $V_A=3$ kV, $V_C=7$ kV, $V_P=3$ kV, 6.7×10^{-6} He.

Although the individual isotopes cannot be resolved, the resolution is adequate for many applications. Preliminary results indicate that single isotope separation is possible if another derivative of the photomultiplier output is taken. Of course, increasing the drift distance for a given ion kinetic energy will also increase resolution. But without a lens to focus the divergent ion trajectories or a means to move the emitter with respect to the channel plates, only a small portion of the entire imaged surface could be examined at one time. If the ion energy could be reduced by setting $V_A \cong 50$ V, travel times in the microsecond range would be obtained with correspondingly improved resolution. This would be possible by replacing the present, simple electrode configuration with one that would permit a smaller ratio of tip to shield potential without image distortion.[17]

As with any instrument employing an electron multiplier for a detector, absolute ion abundances, or even relative ion abundances, cannot be directly inferred from the amplitudes of the ion peaks. This results from the statistical nature of the multiplication process. However, in the present instrument one observes only a 10–15% variation in the amplitude of an ion peak during successive desorption events when the entire desorbed image is monitored. Within this uncertainty the amplitude of a peak resulting from a single ion impact can be deduced by summing the amplitudes of all peaks observed during a single desorption event and dividing by the number of image spots. Assuming that one desorbed layer is produced during each desorption event, and that the detection efficiency for all species is equal, a result of 0.6 mV/single ion impact is obtained.[22] Such a number is difficult to obtain with the conventional atom probe since it provides no information as to the actual number of ions which strike its detector during a single desorption event.

ACKNOWLEDGMENTS

The author wishes to thank D. W. Tipping for his assistance in various phases of instrument construction, F. E. Tentant and the scientific glass facility at Sandia Laboratories for their glass blowing expertise, and J. Abraham and L. Owens of the Bendix Corporation for advice on channel plate operation and a fiber-optics light pipe sample which coupled the photomultiplier to the ion image.

*Supported by the U. S. Atomic Energy Commission.

[1]E. W. Müller and J. A. Panitz, 14th Field Emission Symposium, Washington, D.C., 1967.
[2]E. W. Müller, J. A. Panitz, and S. B. McLane, Rev. Sci. Instrum. **39**, 83 (1968).
[3]E. W. Müller, Ber. d. Bunsenges. **75**, 979 (1971).
[4]S. S. Brenner and J. T. McKinney, Surf. Sci. **23**, 88 (1970).
[5]S. S. Brenner and S. R. Goodman, Scr. Metall. **5**, 865 (1971).
[6]E. W. Müller, Adv. Electron. Electron Phys. **13**, 83 (1960).
[7]As in all other atom probe designs, field evaporation will continue for the duration of the applied pulse unless its nominal amplitude is carefully adjusted so that a field evaporated end-form is reached early in the pulse. The effect of continual evaporation during the applied pulse is to broaden the detected ion peaks and thereby limit resolution unless the evaporation event is terminated in a time shorter than the separation in time of the adjacent species one wishes to resolve. One therefore has two options. Either gently field evaporate to reach an end-form quickly or adjust the pulse duration to be smaller than the required time resolution.
[8]In previous instruments the ion kinetic energy was determined by a dc bias and the amplitude of the evaporation pulse. Their sum had to be increased as the tip radius increased (to maintain a constant evaporation field), requiring constant recalculation to obtain each m/n value. Since each recalculation required another accurate measurement of ion travel time for each species, data reduction time soon became excessive.
[9]Electro-Optical Instruments, Inc., Pasadena, Calif., model CU60/A.
[10]J. A. Panitz, S. B. McLane, and E. W. Müller, Rev. Sci. Instrum. **40**, 1321 (1969).
[11]J. A. Panitz, J. Appl. Phys. **44**, 372 (1973).
[12]CPS, Inc., Sunnyvale, Calif., model 100R.
[13]A product of the Bendix Corp., Electro-Optical Division, Sturbridge, Mass.
[14]J. A. Panitz, Rev. Sci. Instrum. **42**, 724 (1971).
[15]The advantages of using stacked channel plates as a detector in a conventional atom probe were mentioned previously by E. W. Müller, S. V. Krishnaswamy, and S. B. McLane, Rev. Sci. Instrum. **44**, 84 (1973).
[16]Bendix Corp., Electro-Optical Division, Sturbridge, Mass., Chevron CEMA array. Dark current count rate less than 10 counts/sec/cm^2 at gains greater than 10^6.
[17]The ratio of tip to shield potential is restricted by the simple electrode configuration described when atom-by-atom probing is being conducted. For the present instrument, if $V_A \ll 0.1\ (V_C + V_P)$, severe image distortion results and single atomic sites are no longer distinguishable.
[18]In practice, the shield potential during imaging is made as close as possible to $(V_C + V_P)$. This permits the extent of the image shift by the subsequent evaporation pulse to be seen. The detector is positioned over the shifted image spot, the shield potential reduced to V_C, and the desorption pulse, V_P, applied.
[19]S. S. Brenner and J. T. McKinney, Appl. Phys. Lett. **13**, 29 (1968).
[20]A desorption field-ion microscope using a single channel plate and an image intensifier was recently described by R. J. Walko and E. W. Müller, Phys. Status Solidi A **9**, K9 (1972).
[21]J. A. Panitz, Ph.D. thesis, The Pennsylvania State University, 1969.
[22]This number may be too large since the occurrence of possible spurious "after pulses" produced by ion feedback in the multiplier array has been neglected. This problem was recently considered in detail by S. S. Brenner and J. T McKinney, Rev. Sci. Instrum. **43**, 1264 (1972).

Field desorption of helium and neon from tungsten and iridum*

J. A. Panitz

Sandia Laboratories, Albuquerque, New Mexico 87115

(Received 3 September 1974; in final form 10 October 1974)

The first complete crystallographic distribution of helium and neon field adsorbed on tungsten and iridium surfaces has been determined using field desorption mass spectromatry. At 80 K He^+ is removed from tungsten at high work function areas. The absence of He^+ in other regions indicates that either helium is not adsorbed, or that it is removed from the surface as a WHe^{3+} molecular ion during field evaporation of the substrate which is required for He^+ detection. Helium adsorbed on iridium at 80 K may form $IrHe^{3+}$ and neon $IrNe^{2+}$ near prominent zone lines. The absence of ion species in specific crystallographic regions of iridium and tungsten suggests care when interpreting atom probe results in certain metallurgical applications.

INTRODUCTION

The presence of noble gas atoms adsorbed on field-ion emitter surfaces has been clearly established by a number of previous investigations.[1,2] Both theoretical[3] and experimental[4] considerations have localized the position of the noble-gas adsorbate to the apex of each protruding kink-site atom and have identified the adsorption process with a field-induced dipole–dipole interaction. Of particular interest has been the interaction of the inert gas species with its corresponding substrate atom to produce a stable molecular ion,[5] whose appearance can depend on the substrate temperature and the particular crystal region selected for observation.[6]

In this paper we extend the observations of noble-gas adsorption by presenting complete crystallographic distributions of helium and neon adsorbed on tungsten and iridium surfaces and demonstrate how such distributions can reflect the existence of stable molecular ion species. We further suggest that the absence of detected species in specific crystallographic regions may indicate an inhomogeneous ion production at the surface, an effect which must be considered when using the atom-probe in metallurgical applications.

APPARATUS

The ultrahigh-vacuum field-desorption spectrometer used for this study is identical to the one presented previously[7] except that the specimen is both biased and pulsed to eliminate any ambiguity resulting from electron-optical considerations.[8] Crystallographic distributions are obtained by activating the spherical channel electron multiplier array (CEMA) detector coincidently with the arrival of a preselected field-desorbed species and photographically recording the resulting image. By maintaining a very low-evaporation rate (10–100 ions per pulse) and photographically integrating 100 or more evaporation events, a species distribution is obtained which is statistically significant and not influenced by possible trajectory variations resulting from the high ion densities and large changes in surface geometry which accompany large evaporation rates.

Mass resolution and, therefore, the ability to separate adjacent species is essentially determined by the width of the CEMA gate pulse, which in this study, was 28 nsec. Although this is more than sufficient to separate at typical operating potentials He^+ (140 nsec) from

FIG. 1. Integrated desorption image of He^+ from (111) tungsten. 150 events/450 sec, $p=3.1\times10^{-10}$ Torr He, $T=80$ K.

FIG. 2. Integrated desorption image of W^{3+} from (111) tungsten. 100 events/300 sec, $p=4.3\times10^{-10}$ Torr, $T=80$ K.

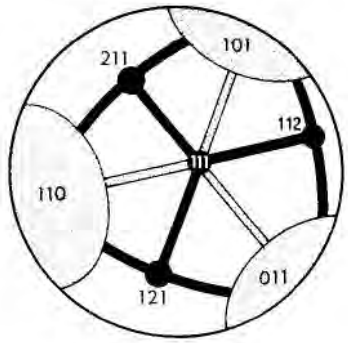

FIG. 3. A schematic summary of Figs. 1 and 2 corresponding to the crystallography displayed by the (111) oriented-tungsten specimen of Fig. 2. Black regions correspond to areas in which the probability of detecting *any* surface species is extremely small. Dotted regions correspond to areas in which WHe^{3+} is most abundant (see text). White regions correspond to areas in which He^+ and W^{3+} are abundant.

Ne^+ (314 nsec) or substrate species, it is not sufficient to unambiguously separate molecular ions from substrate species. Nevertheless, the presence and crystallographic distribution of molecular ions can be deduced by field evaporating the substrate and comparing the resulting inert gas and substrate-desorption micrographs, if one assumes that the inert gas species is adsorbed at all kink-site locations on the surface. The argument is as follows: Since the adsorption of inert gas is owed to a dipole–dipole interaction with the polarized surface atom one would expect that each kink-site atom would eventually adsorb a noble gas species, even in regions of relatively low field.[3] If the substrate is evaporated at a very low rate so that only protruding atoms have a high probability of removal, each kink-site atom will be removed along with its adsorbed inert gas atom as a distinct species or in association with its inert-gas atom as a complex molecular ion. Provided this evaporation rate is maintained during many successive pulses, and the time between pulses made long enough to assure inert gas adsorption at all kink-site locations, the total number of substrate species removed will always equal the number of inert gas species removed, with some inert gas retaining its identity as a distinct species and the rest forming molecules with the substrate. However, because of the width of the gate pulse applied to the detector, the substrate and molecular species cannot be resolved and will appear on the same micrograph. But in regions where molecules are formed, no distinct inert-gas species will be present so that in the inert-gas micrograph regions associated with stable molecular-ion formation will appear dark. Therefore, we will use the following hypothesis in analyzing our data. *Dark regions of the inert gas micrograph which correspond to bright regions in the substrate micrograph indicate areas of stable molecular-ion formation.*

FIG. 5. Integrated desorption image of Ir^{3+}. 100 events/200 sec, $p = 2 \times 10^{-9}$ Torr, $T = 80$ K.

DISCUSSION

Figure 1 is a gated desorption micrograph of He^+ from a (111) oriented tungsten specimen whose corresponding W^{3+} distribution is shown in Fig. 2. A comparison of the micrographs indicates three distinct crystallographic regions of interest, summarized schematically in Fig. 3. First, the relatively low field (110), (101), and (011) regions as well as the vicinity of the zone lines between these regions and the center of the (111) plane are areas in which the probability of formation, and stability, of WHe^{3+} is very high. The relatively few He^+ image spots present in these areas indicate that the probability of formation of a stable molecular ion species is not 100% but is greater than 85%.

Second, the (111) region as well as the zone lines between the (111) and (211), (112), and (121) planes are areas in which there is only a small probability of finding either W^{3+} or He^+. Figure 4, which is a desorption micrograph of Ne^+, further indicates that the probability of finding Ne^+ in these regions is small. These areas of low-relative-ion yield will be considered later.

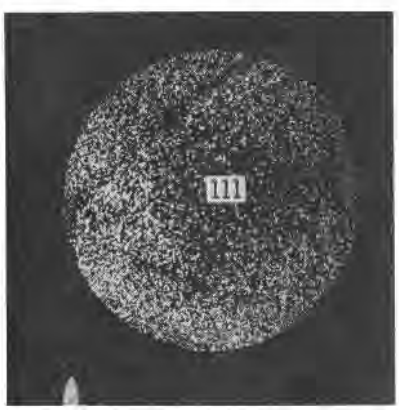

FIG. 4. Integrated desorption image of Ne^+ from (111) tungsten. 150 events/375 sec, $p = 7.2 \times 10^{-10}$ Ne, $T = 80$ K.

FIG. 6. Integrated desorption image of Ir^{3+}. 10 events/100 sec, $p = 7.6 \times 10^{-7}$ Torr He, $T = 80$ K.

FIG. 7. Integrated desorption image of He^+ on (111) iridium. 100 events/200 sec, $p=2\times10^{-9}$ Torr He, $T=80$ K.

The remaining imaged area shows W^{3+}, He^+, and Ne^+ and therefore indicates that molecular ion formation in these regions is not probable, or that the probability of dissociating the molecular species is high.

At 300 K the distribution of W^{3+} shows the same dark regions of Fig. 2 taken at 80 K, but He^+ and Ne^+ are not observed in detectable amounts, so that molecular species are not expected to be present. At 21 K, He^+ is observed on (110)-like planes with high probability, exactly opposite to the 80 K observation of Fig. 1. This suggests that the formation or stability of the molecular species in these regions below 80 K is also negligible.

These observations support the conclusions of an earlier atom-probe examination,[6] in which the crystallographic distribution, stability, and temperature dependence of WHe^{3+} was discussed.

Figures 5 and 6 show the crystallographic distributions of Ir^{2+} and Ir^{3+}, and Figs. 7 and 8 the corresponding He^+ and Ne^+ distributions. A comparison of these figures indicates two main features of interest. First, the vicinity of the zone lines extending from the central (111) plane may be areas in which the formation of stable $IrHe^{3+}$ and $IrNe^{2+}$ is highly probable. Unfortunately, the distribution of these species cannot be examined directly since the former is separated by only 6 nsec from the substrate species and the latter by 33 nsec, which is within the present gate position uncertainty of ±5 nsec. It is possible that these highly localized species have been overlooked in previous high-resolution atom-probe investigations because this technique requires precise positioning of a small probe hole for species detection.

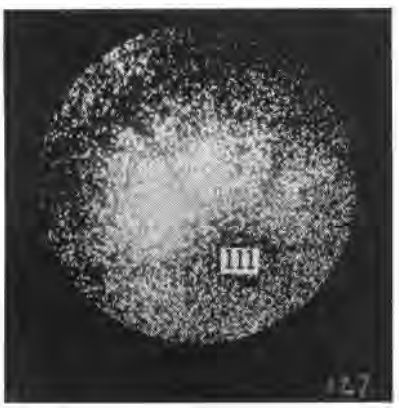

FIG. 8. Integrated desorption image of Ne^+ on (111) iridium. 10 events/100 sec, $p=2\times10^{-9}$ Torr Ne, $T=80$ K.

Second, there are dark regions which are coincident in the Ir^{2+}, Ir^{3+}, He^+, and Ne^+ micrographs again indicating specific regions of the surface having low relative-ion yield. As in the case of tungsten, these regions are retained at 300 K and at 80 K even in the presence of 7×10^{-7} Torr of helium. Such dark regions have also been seen in nongated desorption images of Pt[9] and W[10] and appear to be characteristic of the metals used in field-ion microscopy. Although the low ion yield in these regions may be explainable in terms of simple trajectory[11] or magnification[12] considerations, or require a more unorthodox explanation such as ion neutralization at the surface,[13] it must be considered in all atom-probe determinations of species distribution. The atom-probe technique relies, for positioning its small probe hole, on an inert-gas ion image which does not directly indicate regions of low ion yield. Although not previously appreciated, it is apparent that the variation in detected ion yield over the surface, which appears to be independent of the actual species distribution either adsorbed on the surface or distributed in the bulk, can significantly alter absolute compositional profile interpretations.[14] The clue to possible problem regions, when using the atom probe, is an area of increased regional brightness in the ion image which seems, at least for the metals we have examined, to be uniquely associated with areas of low ion yield during desorption.

[1]E. W. Müller, S. B. LcMane, and J. A. Panitz, Surf. Sci. **17**, 430 (1969).
[2]J. T. McKinney and S. S. Brenner, Sixteenth Field Emission Symposium, Pittsburgh, PA, 1969.
[3]R. T. Tsong and E. W. Müller, J. Chem. Phys. **55**, 2884 (1971).
[4]E. W. Müller and S. V. Krishnaswamy, Surf. Sci. **36**, 29 (1973).
[5]E. W. Müller, S. V. Krishnaswamy, and S. B. McLane, Surf. Sci. **23**, 112 (1970).
[6]E. W. Müller, S. V. Krishnaswamy, and S. B. McLane, Phys. Rev. Lett. **31**, 1282 (1973).
[7]J. A. Panitz, J. Vac. Sci. Technol. **11**, 206 (1974).
[8]J. A. Panitz, S. B. McLane, and E. W. Müller, Rev. Sci. Instrum. **40**, 1321 (1969).
[9]E. W. Müller and T. T. Tsong, Prog. Surf. Sci. **4**, Part I, 48 (1973).
[10]A. J. W. Moore and J. A. Spink; A. R. Waugh, E. D. Boyes, D. A. Coppell, A. Watts, and M. J. Southon, 21st Field Emission Symposium, Marseille, France, 1974.
[11]E. W. Müller, 15th Field Emission Symposium, Bonn, Germany, 1968; J. A. Panitz, Ph.D. dissertation, The Pennsylvania State University, 1969.
[12]E. W. Müller, private communication.
[13]J. A. Panitz, Seminar at the National Bureau of Standards, Gaithersburg, Maryland, 1974. The origin of the low ion yields will be discussed in detail in a future publication.
[14]To minimize this difficulty, one should always measure the relative abundance of substrate and impurity, or substrate and adsorbate as a function of crystallographic orientation.